Label-Free Quantitative Imaging of Cholesterol in Intact Tissues by Hyperspectral Stimulated Raman Scattering Microscopy**

Ping Wang, Junjie Li, Pu Wang, Chun-Rui Hu, Delong Zhang, Michael Sturek, and Ji-Xin Cheng**

Cholesterol is an indispensable structural constituent of membranes, and it also plays a prominent role in the biosynthesis of steroid hormones. Excessive cholesterol storage is a hallmark of atherosclerotic cardiovascular diseases. Crystalline cholesterol has not only been found in advanced atherosclerotic lesions,[1] but it has also been recognized as an inflammatory stimulus that appears in a very early stage of atherosclerosis.[1c,d,2] Abnormal storage of cholesterol also occurs in steroidogenic cells[3] and Niemann–Pick type C disease.[4] However, quantitative imaging of cholesterol and its esterified form in an intact biological tissue remains a challenge. The widely applied histological hematoxylin and eosin staining only allows indirect mapping of crystalline cholesterol clefts.[1a] Lipid-soluble Sudan dyes, such as Oil Red O and Bromine-Sudan black, are widely used to stain neutral lipid droplets that contain the cholesteryl ester and triglyceride,[5] but these dyes neither stain crystalline cholesterol, nor elucidate the composition of lipid droplets. Filipin is a gold standard for staining free cholesterol in fixed cells, but is unable to label either large cholesterol crystals or lipid droplets that contain the cholesteryl ester.[6] Confocal laser reflection microscopy[2,7] and micro-optical coherence tomography[8] have been successfully implemented to visualize reflective substances such as cholesterol and silica, but neither has the capability for chemical identification.

Spontaneous Raman spectroscopy is an established method for imaging cholesterol and other biochemicals in isolated cells or tissue samples in a label-free manner,[9] but it suffers from a slow imaging process and strong background auto-fluorescence. Nonlinear coherent Raman microscopy,[10] which is based on coherent anti-Stokes Raman scattering

(CARS)[11] and stimulated Raman scattering (SRS),[12] significantly improved the image-acquisition speed. Furthermore, multiplex/hyperspectral CARS[13] and hyperspectral SRS[14] have been developed to resolve spectrally overlapping Raman bands, and they have been employed to map cholesterol in atherosclerotic plaques.[13e,g,14a] To date, CARS and SRS imaging of cholesterol has predominantly focused on the carbon–hydrogen (C−H) stretching region where lipids exhibit strong vibrational signals. Nevertheless, quantitative identification of free and esterified cholesterol from other lipids using the C−H stretching bands is difficult, because these bands are highly crowded and spectrally overlapped in the spectral window of 2800–3100 cm^{-1}.[14a,15] Furthermore, these overlapping C−H stretching bands were shown to exhibit varied dependence on the excitation polarization, even when they are obtained from the same molecule,[14a] which renders quantitative mapping especially difficult.

Herein, we demonstrate the label-free quantitative imaging of cholesterol storage in intact atherosclerotic arterial tissues by the detection of fingerprint Raman bands with a hyperspectral SRS microscope (Supporting Information, Figure S1). In particular, we employed the sterol C=C band at 1669 cm^{-1} as a characteristic band of cholesterol. Other significant Raman bands in the same spectral window, including the acyl C=C band, the ester C=O band, and the amide I band, were recorded simultaneously. Quantitative chemical maps of each chemical group were generated by multivariate curve resolution (MCR)[16] analysis (Supporting Information, Figure S2). Hyperspectral SRS imaging and multivariate analysis in the fingerprint region, as reported here, may lead to new research opportunities by providing chemical maps of key molecules in intact cells and tissues.

We first demonstrated the feasibility of our method by SRS imaging of a mixture of crystalline cholesterol, glyceryl trioleate, and bovine serum albumin (BSA) powder, and their molecular structures are shown in Figure 1a. As indicated, each glyceryl trioleate molecule contains a total of three *cis* C=C bonds (herein referred to as acyl C=C bonds) in the three lipid acyl chains, and each cholesterol comprises one C=C bond (referred to as the sterol C=C bond) in the ring. Importantly, these two types of C=C bonds are spectrally separated in the Raman spectrum, with peaks at 1655 cm^{-1} for the acyl C=C bond and 1669 cm^{-1} for the sterol C=C bond, respectively (Figure 1b). In the same spectral region, BSA, a protein representative, gives a broad amide I band. As these Raman bands have either different peak positions or exhibit different profiles, selective mapping of triglyceride, cholesterol, and protein is possible through hyperspectral SRS imaging and MCR analysis. A hyperspectral stack of 60

[*] Dr. P. Wang, P. Wang, C. Hu, Prof. J.-X. Cheng
Weldon School of Biomedical Engineering, Purdue University
West Lafayette, IN 47906 (USA)
E-mail: jcheng@purdue.edu

J. Li
Department of Biological Sciences, Purdue University (USA)

D. Zhang
Department of Chemistry, Purdue University (USA)

Prof. M. Sturek
Department of Cellular and Integrative Physiology
Indiana University Medical School
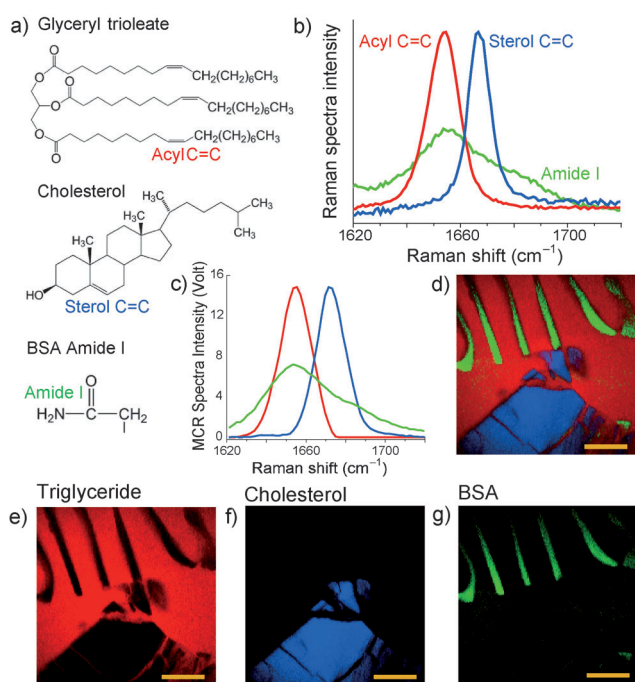Indianapolis, IN 46202 (USA)
E-mail: msturek@iu.edu

Figure 1. Hyperspectral SRS imaging and MCR analysis of a mixture of cholesterol, triglyceride, and BSA. a) Chemical structures of glyceryl trioleate, cholesterol, and BSA. The acyl C=C and the sterol C=C bond and the amide I group are indicated. b) Spontaneous Raman spectra with a spectral window of 1620–1720 cm^{-1} for triglyceride (——), cholesterol (——), and BSA (——). c) Output spectra from hyperspectral SRS imaging and MCR analysis of triglyceride (——), cholesterol (——), and BSA (——). d) Color overlay image produced by combining images (e)–(g), which are concentration maps that were retrieved by MCR of triglyceride (liquid), crystalline cholesterol, and BSA (powder). Scale bar: 50 μm.

images at wavenumbers ranging from 1620 to 1720 cm^{-1} was obtained with a total acquisition time of less than 40 s (Supporting Information, Movie S1). The X-Y-Ω image stack was analyzed with an MCR algorithm, which retrieved both the spectra and concentration maps that correspond to glyceryl trioleate, cholesterol, and BSA.[14f] Figure 1 c shows the spectra optimized by MCR for each component, which match the spontaneous Raman spectra shown in Figure 1 b. The reconstructed concentration maps of glyceryl trioleate, cholesterol, and BSA are presented in Figure 1 e–g, and the overlay image is shown in Figure 1 d. These data collectively demonstrate the applicability of SRS microscopy and MCR analysis for mapping biomolecules of overlapped Raman bands.

We further developed a strategy for the quantification of cholesterol storage in lipid droplets. Under realistic biological circumstances, excess cholesterol exists either as crystalline cholesterol or in the esterified version, in which an acyl chain is linked to the cholesterol through an ester bond. Cholesteryl ester is usually mixed with triglyceride and stored in lipid droplets. Quantifying the molar percentage of cholesteryl ester in lipid droplets is important to evaluate cholesterol metabolism. Although the peaks of the acyl and sterol C=C bands are separated, a triglyceride molecule contains various amounts of acyl C=C bonds in its three acyl chains, depending

on the degree of unsaturation. Moreover, the cholesteryl ester may contain zero (in cholesteryl palmitate), one (in cholesteryl oleate), or two (in cholesteryl linoleate) acyl C=C bonds in its acyl chain. Therefore, it is difficult to use the C=C bonds alone to quantify the molar percentage of cholesteryl ester in a lipid droplet. To address this difficulty, we developed a new strategy for cholesteryl ester quantification by counting the ester C=O bond, which gives a Raman band that peaks at 1745 cm^{-1}. Triglyceride molecules contain three ester C=O bonds that link glycerol to three acyl chains (Figure 1 a). Meanwhile, each cholesteryl ester molecule contains one sterol ring and one acyl chain that are linked by one ester C=O bond. Given that y is the molar fraction of cholesteryl ester in a triglyceride/cholesteryl ester mixture, and x is the measured concentration ratio of sterol C=C to C=O, we can derive the following equation:

$$x = y/(y + 3(1-y)) \tag{1}$$

Here, $3(1-y)$ is the relative concentration of C=O bonds in triglyceride. Based on Eq. (1), the molar fraction of cholesteryl ester is:

$$y = 3x/(1 + 2x) \tag{2}$$

Thus, if we perform hyperspectral SRS imaging and MCR analysis of acyl C=C, sterol C=C, and the ester C=O bonds, the above model will enable us to calculate the molar fraction of cholesteryl ester in a mixture. Moreover, the degree of unsaturation of the lipid droplet can be evaluated as the concentration ratio of acyl C=C to C=O.

To experimentally validate the above strategy, we performed hyperspectral SRS imaging of emulsions that were composed of known molar ratios of glyceryl trioleate, as a triglyceride representative, and cholesteryl oleate, as a cholesteryl ester representative. The spectral window covered a Raman shift of 1620–1800 cm^{-1} for the quantitative imaging of acyl C=C, ester C=O, and sterol C=C bonds. The corresponding SRS spectra were recorded from pure glyceryl trioleate and pure crystalline cholesterol (Figure 2 a). The ester C=O band was found to be 5.4 times weaker in amplitude than the C=C band, and has a separated single peak at 1745 cm^{-1}. Hyperspectral SRS imaging of emulsions with various molar ratios of glyceryl trioleate to cholesteryl oleate produced spectra for all emulsions as shown in Figure 2 b. With an increasing percentage of cholesteryl oleate in emulsion, the SRS spectra exhibited a transition from a single narrow peak of the acyl C=C bond (1655 cm^{-1}, full width at half maximum (FWHM) = 17 cm^{-1}) to an overlapped peak that consists of both acyl and sterol C=C bands. In an emulsion of pure cholesteryl oleate, which contains one acyl and one sterol C=C bond, we observed a relatively broad Raman band with contributions from the acyl C=C and sterol C=C bands at equal intensity (Dashed line in Figure 2 b). Such spectral profiles were confirmed by spontaneous Raman spectroscopy (Supporting Information, Figure S3). To quantify the percentage of cholesteryl ester in mixed emulsions, hyperspectral SRS spectra of emulsions and the standard SRS spectra of acyl C=C, sterol C=C, and C=O bonds were used as inputs for the MCR algorithm, serving as
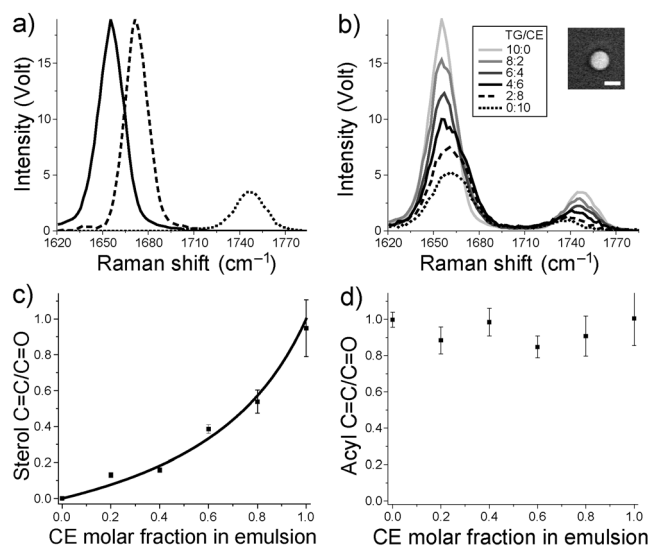
Figure 2. Quantification of the molar percentage of cholesteryl ester in a lipid emulsion. a) SRS spectra of the acyl C=C (——), sterol C=C (– – –), and ester C=O (•••••) bonds. b) SRS spectra of emulsions composed of glyceryl trioleate and cholesteryl oleate at molar ratios of 10:0, 8:2, 6:4, 4:6, 2:8, and 0:10. Spectra were obtained from the averaging of spectra in 100 pixels for each emulsion. Inset: SRS image of an emulsion at TG/CE = 8:2. Scale bar: 5 μm. c) MCR quantification (■) of the molar fraction of cholesteryl ester in emulsion, and values calculated (——) using Eq. (1). d) Unsaturation degree of emulsions measured by MCR. CE = cholesteryl ester, TG = triglyceride.

Figure 3. Hyperspectral SRS imaging and MCR analysis of an atherosclerotic artery. a–c) Reconstructed concentration images of crystallized free cholesterol (yellow), lipid droplets (green), and protein background (cyan). d) Overlay image of (a)–(c). Scale bars: 20 μm. e) MCR output spectra of crystalline cholesterol (——), lipid droplets (——), and protein (——); SRS spectra of acyl C=C (•••••) and sterol C=C bonds (•••••).

a data matrix and initial spectra estimation, respectively. The concentration ratio between the sterol C=C and the C=O bonds were plotted as a function of the actual cholesteryl ester percentage in each emulsion (Figure 2c). These results are in good agreement with the calculation based on Eq. (1). By calculating the concentration ratio of acyl C=C to C=O, MCR quantification also provided the degree of lipid unsaturation for all emulsions (Figure 2d). The degree of unsaturation is close to 1.0 for all emulsions. This result is consistent with the composition of the emulsions in which both cholesteryl oleate and glyceryl trioleate were mono-unsaturated. These results collectively established an approach for quantifying the percentage of cholesteryl ester and the degree of unsaturation in a lipid droplet based on SRS imaging of C=O and C=C bonds. The Raman shift of the ester C=O bond slightly varied with the percentage of cholesteryl ester (Figure 2b). However, as a soft-modeling approach[17], MCR allowed the treatment of varying spectra in data sets and the derivation of correct concentration profiles.

Once this method had been established through phantom studies, we further demonstrated quantitative concentration mapping of crystalline cholesterol, lipid droplets, and proteins in intact arteries harvested from an atherosclerotic pig. An X-Y-Ω image stack was recorded in the fingerprint range of 1620–1800 cm^{-1} (Supporting Information, Movie S2). This stack was then decomposed into concentration maps of crystalline cholesterol, lipid, and protein (Figure 3a–c). The overlay of the three maps is shown in Figure 3d. Specifically, Figure 3a demonstrates the reconstructed concentration map of crystalline cholesterol that formed in the atherosclerotic
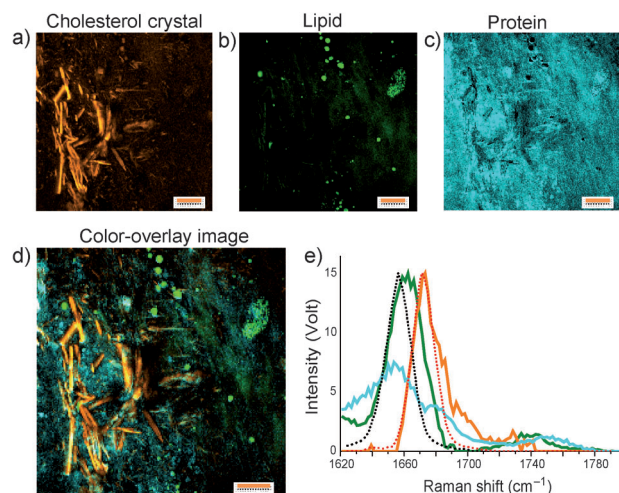
plaque. The corresponding MCR optimized spectrum of the sterol C=C band entails a peak at 1669 cm^{-1} (Figure 3e), which is in accordance with the SRS spectrum recorded from pure crystalline cholesterol. Abundant needle-like cholesterol crystals are recognized in the reconstructed image. The capability to identify such structures is important, because cholesterol crystallization is recognized to be a major determinant of plaque rupture in acute coronary syndrome.[1b] Figure 3b presents the map of lipid droplets; the corresponding spectrum obtained by MCR is shown in Figure 3e. Compared with the Raman spectrum of the acyl C=C bond in pure glyceryl trioleate, the lipid spectrum exhibited a significantly broadened profile towards higher wavenumbers, which implies that these lipid droplets contain a significant amount of cholesteryl ester. Figure 3c shows the concentration image of protein, which is ubiquitous, but more concentrated in cholesterol-crystal-rich areas. Taken together, the MCR analysis allowed distinctive mapping of lipid droplets that are rich in cholesteryl ester, crystalline cholesterol, and protein in an intact atherosclerotic artery.

Using the strategy shown in Figure 2, we further quantified the molar fraction of cholesteryl ester and the degree of unsaturation for the lipid droplets in the atherosclerotic artery. Figure 4a shows an area with abundant lipid droplets, distributed protein, and a few cholesterol crystals. To quantify the amount of cholesteryl ester in these lipid droplets, concentration maps of acyl C=C, sterol C=C, and ester C=O bonds (Figure 4b–d) were reconstructed from the hyperspectral SRS stack (Supporting Information, Movie S3), and the SRS spectra of the pure components are shown in Figure 2a. The corresponding spectra that were optimized by MCR are shown in Figure 4e. Compared to the input spectrum, the C=O band is slightly shifted to lower wavenumbers because of the presence of cholesteryl ester in the lipid droplets.
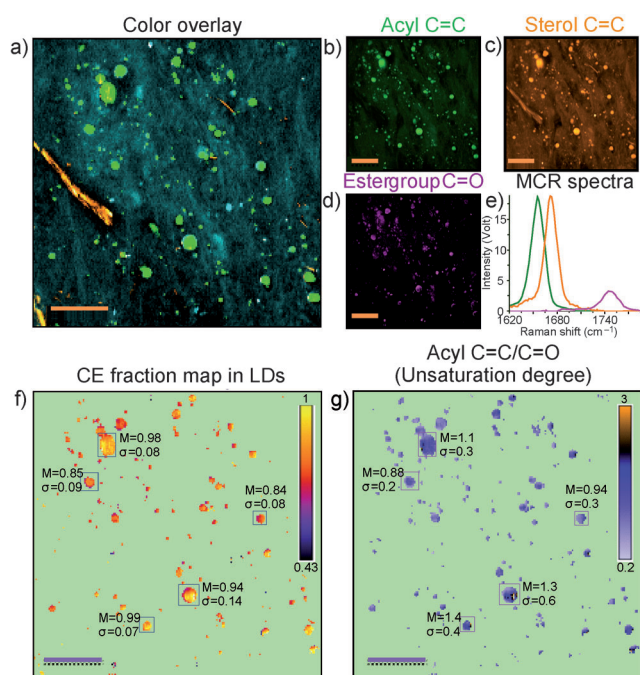
Figure 4. MCR quantification of the cholesteryl ester level and degree of unsaturation in lipid droplets of an intact atherosclerotic artery. a) Overlay map of crystalline cholesterol (yellow), lipid droplets (green), and protein (cyan). b–d) Concentration maps of acyl C=C, sterol C=C, and ester C=O bonds reconstructed by MCR. e) MCR output spectra corresponding to maps (b)–(d); acyl C=C (———), sterol C=C (———), and ester C=O (———) bonds. f) Image of lipid droplets based on the molar fraction of cholesteryl ester in each lipid droplet. The calibrated cholesteryl ester level is shown for some lipid droplets. g) Image of lipid droplets based on the ratio between the concentration of acyl C=C and ester C=O bonds. The degree of unsaturation is shown for some lipid droplets. Scale bars: 20 μm. M = mean value of the cholesteryl ester percentage, σ = standard deviation.

We then used the map of the ester C=O bond as an internal standard to normalize maps of both acyl C=C and sterol C=C bonds. The ratio between the maps of those two bonds (sterol C=C/C=O) represents the number of sterol C=C bonds per fatty acid chain. According to Eq. (2), a map of the molar fraction of cholesteryl ester was obtained (Figure 4 f). The mean cholesteryl ester level (M) and its standard deviation (σ) are given for indicated areas. Our data show that cholesteryl ester is highly abundant in the lipid droplets in the imaged area. The ratio between the maps of acyl C=C and ester C=O bonds reflects the unsaturation degree of the lipid droplets (Figure 4 g). The unsaturation degrees measured for the indicated lipid droplets are close to 1.0. This result is consistent with previous results that indicated that cholesteryl oleate is the major component inside the lipid droplets of atherosclerotic arteries.[18] These results show that hyperspectral SRS and MCR are capable of compositional analysis of lipid droplets in intact biological specimens.

[1] a) G. S. Abela, K. Aziz, A. Vedre, D. R. Pathak, J. D. Talbott, J. DeJong, *Am. J. Cardiol.* **2009**, *103*, 959; b) Z. Chen, M. Ichetovkin, M. Kurtz, E. Zycband, D. Kawka, J. Woods, X. He, A. S. Plump, E. Hailman, *Lipids Health Dis.* **2010**, *9*, 61; c) K. Rajamäki, J. Lappalainen, K. Öörni, E. Välimäki, S. Matikainen, P. T. Kovanen, K. K. Eklund, *Plos One* **2010**, *5*, e11765; d) G. S. Abela, *J. Clin. Lipidol.* **2010**, *4*, 156.
[2] P. Duewell et al., *Nature* **2010**, *464*, 1357; see the Supporting Information.
[3] a) J. Hu, Z. Zhang, W. J. Shen, S. Azhar, *Nutr. Metab.* **2010**, *7*, 47; b) F. B. Kraemer, V. K. Khor, W. J. Shen, S. Azhar, *Mol. Cell. Endocrinol.* **2013**, *371*, 15.
[4] M. T. Vanier, *Orphanet J. Rare Dis.* **2010**, *5*, 16.
[5] C. M. van Gent, J. J. Emeis, *Prog. Biochem. Pharmacol.* **1977**, *13*, 262.
[6] D. Hirsch, R. Azoury, S. Sarig, H. S. Kruth, *Calcif. Tissue Int.* **1993**, *52*, 94.
[7] V. Hornung, F. Bauernfeind, A. Halle, E. O. Samstad, H. Kono, K. L. Rock, K. A. Fitzgerald, E. Latz, *Nat. Immunol.* **2008**, *9*, 847.
[8] L. Liu, J. A. Gardecki, S. K. Nadkarni, J. D. Toussaint, Y. Yagi, B. E. Bouma, G. J. Tearney, *Nat. Med.* **2011**, *17*, 1010.
[9] A. Lattermann, C. Matthaus, N. Bergner, C. Beleites, B. F. Romeike, C. Krafft, B. R. Brehm, J. Popp, *J. Biophotonics* **2013**, *6*, 110.
[10] J. X. Cheng, X. S. Xie, *Coherent Raman Scattering Microscopy*, Taylor & Francis Group, New York, **2012**.
[11] a) M. D. Duncan, J. Reintjes, T. J. Manuccia, *Opt. Lett.* **1982**, *7*, 350; b) A. Zumbusch, G. R. Holtom, X. S. Xie, *Phys. Rev. Lett.* **1999**, *82*, 4142; c) J.-X. Cheng, X. S. Xie, *J. Phys. Chem. B* **2004**, *108*, 827; d) V. Andreas, *J. Phys. D* **2005**, *38*, R59; e) L. G. Rodriguez, S. J. Lockett, G. R. Holtom, *Cytometry Part A* **2006**, *69*, 779; f) M. Müller, A. Zumbusch, *ChemPhysChem* **2007**, *8*, 2156; g) T. Hellerer, C. Axang, C. Brackmann, P. Hillertz, M. Pilon, A. Enejder, *Proc. Natl. Acad. Sci. USA* **2007**, *104*, 14658; h) C. L. Evans, X. S. Xie, *Annu. Rev. Anal. Chem.* **2008**, *1*, 883; i) J. P. Pezacki, J. A. Blake, D. C. Danielson, D. C. Kennedy, R. K. Lyn, R. Singaravelu, *Nat. Chem. Biol.* **2011**, *7*, 137; j) E. Bélanger, F. P. Henry, R. Vallée, M. A. Randolph, I. E. Kochevar, J. M. Winograd, C. P. Lin, D. Côté, *Biomed. Opt. Express* **2011**, *2*, 2698; k) M. Paar et al., *J. Biol. Chem.* **2012**, *287*, 11164; see the Supporting Information.
[12] a) E. Ploetz, S. Laimgruber, S. Berner, W. Zinth, P. Gilch, *Appl. Phys. B* **2007**, *87*, 389; b) C. W. Freudiger, W. Min, B. G. Saar, S. Lu, G. R. Holtom, C. W. He, J. C. Tsai, J. X. Kang, X. S. Xie, *Science* **2008**, *322*, 1857; c) P. Nandakumar, A. Kovalev, A. Volkmer, *New J. Phys.* **2009**, *11*, 033026; d) B. G. Saar, C. W. Freudiger, J. Reichman, C. M. Stanley, G. R. Holtom, X. S. Xie, *Science* **2010**, *330*, 1368; e) D. Zhang, M. N. Sipchenko, J. X. Cheng, *J. Phys. Chem. Lett.* **2011**, *2*, 1248; f) W. Min, C. W. Freudiger, S. Lu, X. S. Xie, *Annu. Rev. Phys. Chem.* **2011**, *62*, 507; g) J. Moger, N. L. Garrett, D. Begley, L. Mihoreanu, A. Lalatsa, M. V. Lozano, M. Mazza, A. Schatzlein, I. Uchegbu, *J. Raman Spectrosc.* **2012**, *43*, 668; h) T. Lee, H. Mundoor, D. G. Gann, T. J. Callahan, I. I. Smalyukh, *Opt. Express* **2013**, *21*, 12129; i) J. C. Mansfield, G. R. Littlejohn, M. P. Seymour, R. J. Lind, S. Perfect, J. Moger, *Anal. Chem.* **2013**, *85*, 5055; j) L. Wei, Y. Yu, Y. Shen, M. C. Wang, W. Min, *Proc. Natl. Acad. Sci. USA* **2013**, *110*, 11226.
[13] a) J.-X. Cheng, A. Volkmer, L. D. Book, X. S. Xie, *J. Phys. Chem. B* **2002**, *106*, 8493; b) M. Müller, J. M. Schins, *J. Phys. Chem. B* **2002**, *106*, 3715; c) H. A. Rinia, K. N. J. Burger, M. Bonn, M. Müller, *Biophys. J.* **2008**, *95*, 4908; d) M. Bonn, M. Müller, H. A.

Rinia, K. N. J. Burger, *J. Raman Spectrosc.* **2009**, *40*, 763; e) S. H. Kim, E. S. Lee, J. Y. Lee, B. S. Lee, J. E. Park, D. W. Moon, *Circul. Res.* **2010**, *106*, 1332; f) P. D. Chowdary, W. A. Benalcazar, Z. Jiang, D. M. Marks, S. A. Boppart, M. Gruebele, *Anal. Chem.* **2010**, *82*, 3812; g) R. S. Lim, J. L. Suhalim, S. Miyazaki-Anzai, M. Miyazaki, M. Levi, E. O. Potma, B. J. Tromberg, *J. Lipid Res.* **2011**, *52*, 2177; h) C. Y. Lin, J. L. Suhalim, C. L. Nien, M. D. Miljkovic, M. Diem, J. V. Jester, E. O. Potma, *J. Biomed. Opt.* **2011**, *16*, 021104; i) S. Bégin, B. Burgoyne, V. Mercier, A. Villeneuve, R. Vallée, D. Côté, *Biomed. Opt. Express* **2011**, *2*, 1296; j) Y. J. Lee, D. Moon, K. B. Migler, M. T. Cicerone, *Anal. Chem.* **2011**, *83*, 2733; k) A. F. Pegoraro, A. D. Slepkov, A. Ridsdale, D. J. Moffatt, A. Stolow, *J. Biophotonics* **2013**, DOI: 10.1002/jbio.201200171.

[14] a) J. L. Suhalim, C.-Y. Chung, M. B. Lilledahl, R. S. Lim, M. Levi, B. J. Tromberg, E. O. Potma, *Biophys. J.* **2012**, *102*, 1988; b) Y. Ozeki, W. Umemura, Y. Otsuka, S. Satoh, H. Hashimoto, K. Sumimura, N. Nishizawa, K. Fukui, K. Itoh, *Nat. Photonics* **2012**, *6*, 844; c) D. Fu, F.-K. Lu, X. Zhang, C. Freudiger, D. R. Pernik, G. Holtom, X. S. Xie, *J. Am. Chem. Soc.* **2012**, *134*, 3623; d) L. J. Kong, M. B. Ji, G. R. Holtom, D. Fu, C. W. Freudiger, X. S. Xie, *Opt. Lett.* **2013**, *38*, 145; e) J. Mansfield, J. Moger, E. Green, C. Moger, C. P. Winlove, *J. Biophotonics* **2013**, DOI: 10.1002/jbio.201200213; f) D. Zhang, P. Wang, M. N. Slipchenko, D. Ben-Amotz, A. M. Weiner, J. X. Cheng, *Anal. Chem.* **2013**, *85*, 98.

[15] Z. Movasaghi, S. Rehman, I. U. Rehman, *Appl. Spectrosc. Rev.* **2007**, *42*, 493.

[16] J. Jaumot, R. Gargallo, A. de Juan, R. Tauler, *Chemom. Intell. Lab.* **2005**, *76*, 101.

[17] A. de Juan, M. Maeder, M. Martinez, R. Tauler, *Chemom. Intell. Lab.* **2000**, *54*, 123.

[18] C. Degirolamo, G. S. Shelness, L. L. Rudel, *J. Lipid Res.* **2009**, *50*, S434.